Iranian Journal of Physics Research, Vol. 25, No. 3, 2025
DOI: 10.47176/ijpr.25.1.12040

Tuning the structural, electronic, magnetic, and optical properties of EuS via Nd^{2+} doping: a comprehensive study

Kamal Kishor Dwivedi[1], Anuj kumar[2], U.C. Srivastava[3], Aman Kumar[4*] and Shyamendra Pratap Singh[5*]
[1]Department of Physics, Dr. Shivanand Nautiyal Govt P.G. College Karnprayag Uttarakhand, India.
[2]Department of Physics, Mahamaya Government Degree College, Sherkot, Bijnor, Uttar Pradesh, India.
[3]Department of Physics, Amity Institute of Applied Sciences, Amity University, Noida-201301, India
[4]Department of Physics, KVSCOS, Swami Vivekanand Subharti University, Meerut-250005, India.
[5]Department of Physics, Swami Vivekanand Govt P.G. College Lohaghat Uttarakhand, India.

*Corresponding Author- 01amankumar@gmail.com, spsingh.sps21@gmail.com

(Received 13 January 2025 ; in final form 19 March 2025)

Abstract
This study employs first-principles density functional theory (DFT) calculations within the WIEN2K software framework to investigate the electronic, magnetic, and optical properties of EuS and $Eu_{0.5}Nd_{0.5}S$ compounds. The computational methodology incorporates the Tran-Blaha modified Becke-Johnson (TB-mBJ) exchange-correlation potential to enhance the accuracy of electronic structure predictions. Structural parameters, including equilibrium lattice constants and unit cell volumes, were derived by fitting the total energy versus volume data to the Birch-Murnaghan equation of state (BME). The computed structural properties exhibit strong agreement with available experimental data, validating the reliability of the adopted computational approach. Electronic properties were examined via band structure (BS) calculations, supplemented by an in-depth analysis of the total and partial density of states (T-DOS and P-DOS). The band structure results confirm the metallic nature of both EuS and $Eu_{0.5}Nd_{0.5}S$, as indicated by the presence of conduction states at the Fermi level. Optical properties were systematically analyzed through key frequency-dependent response functions, including the real and imaginary components of the dielectric function [$\varepsilon_1(\omega)$ and $\varepsilon_2(\omega)$], reflectivity spectrum [$R(\omega)$], energy-loss function [$L(\omega)$], refractive index [$n(\omega)$], and absorption coefficient [$\alpha(\omega)$]. These optical parameters elucidate the interaction mechanisms between these materials and electromagnetic radiation, offering crucial insights into their potential applications in optoelectronic and photonic technologies.

Keywords: WIEN2K, Optical Properties, Chalcogenides, GGA.

1. Introduction

Rare earth compounds possess intricate electrical characteristics associated with strongly coupled f-electrons, making them particularly intriguing to researchers in both experimental and theoretical domains. Numerous rare earth elements exist as trivalent ions in the solid state, however, mostly exhibit a divalent state in their atomic form. All elemental rare earths are trivalent, with the exception of Eu and Yb, which are divalent. Compounds containing europium may exhibit divalent or trivalent configurations. The bulk of pnictides and europium chalcogenides crystallise in the simple NaCl crystal structure, creating a series that is quite uncomplicated to investigate using first principles theory. Chalcogenides have attracted considerable attention recently due to their potential use in spin filtering and spintronic devices [1-2].

The intricate electrical characteristics of rare earth compounds have garnered significant experimental and theoretical attention, particularly concerning the tightly correlated f-electrons. Your study elucidates the fascinating properties of europium chalcogenides and their potential use in spintronic devices. Understanding the differences between the divalent and trivalent states of europium is crucial, since these variances influence the compounds' electrical and magnetic characteristics. There are several parallels between the crystal structures of sodium chloride and europium chalcogenides. This facilitates first-principles computations and enhances the precision of electronic structure models. This class possesses appealing mechanical properties, including high oxidation resistance, stiffness, strength, ductility, and elevated temperature performance. Rare earth intermetallics, which incorporate rare earth and transition elements, have been extensively researched for several decades [3]. This renders them ideal structural materials for high-temperature applications in the automotive, aviation, and aerospace sectors. In the context of

spintronic application development, it is essential to emphasise EuO as a ferromagnetic semiconductor characterised by strongly spin-polarized carriers. Notwithstanding EuS low critical temperature (Tc), the significant magnetoresistance of the Gd/EuS/Al hybrid device underscores the material's potential use as a spin filter. This limitation is a common issue in the industry, prompting more investigation into the electrical and magnetic characteristics of alternative Eu-chalcogenides that may possess enhanced features. An essential element of your study is the conventional treatment of f electrons as localised, in contrast to the mobility nature of s, p, and d electrons. The behaviour of f-electrons may significantly affect the overall electrical configuration and magnetic properties. By accurately considering electron correlations, methods such as TB-mBJ or GGA + U may enhance comprehension. Utilising two separate theories to explain the behaviour of electrons inside a single substance is inadequate. Recently, researchers have used the TB-mBJ method inside density functional theory (DFT). This method has shown efficacy in uniformly treating all electrons in rare earth minerals [4-5]. The energy required to localise an f-electron is quantified by the self-interaction correction. The f-configuration of the rare earth ion remains stable provided that the localisation energy equals the energy acquired by an electron via hybridisation with the conduction band states. Altering the ambient factors readily adjusts the very sensitive energy equilibrium.

2-Computational Methodology

The crystal structure of EuS resembles that of NaCl, exhibiting cubic symmetry and belonging to the space group Fm3¯m (225). Conversely, Eu0.5Nd0.5S exhibits a tetragonal structure characterised by the space group P4/mmm (123). The lattice constants for EuS are $a_0=b_0=c_0=5.968$ Å, while $Eu_{0.5}Nd_{0.5}S$ has $a_0=b_0=7.44$ Å and $c_0=10.53$ Å. We used the TB-mBJ potential inside the full-potential linearised augmented plane wave (FP-LAPW) approach, with the WIEN2K code [6], to get our findings. The TB-mBJ technique is a widely used density functional theory (DFT) approach for determining electron structures. It enhances the accuracy of predictions for electrical and magnetic characteristics [7–11]. We used an 8×8×8 k-point mesh for Brillouin zone sampling. This selection optimises computing efficiency while ensuring the precision necessary for dependable electrical structure computations, including band structure, density of states, and total energy assessments. In instances of convergence or k-point sensitivity problems, a more refined mesh may be used. Furthermore, we included one local orbital for the initial vacant s, p, d, and f states for each atom to augment the basis set [12]. We used the Murnaghan equation of state [13] to fit the total energies acquired at different lattice constants in order to ascertain the bulk modulus and the optimised lattice constants. We examined other aspects beyond the structural features of the $Eu_{0.5}Nd_{0.5}S$ series. We specifically compared the electrical structures to experimental data typically gathered at ambient temperature. We used a customised approach to assess the magnetic characteristics of the materials [14].

2.1-Structral and Electronic Properties

Figure 1(a, b) illustrates the structural properties in terms of unit cell structure of EuS and $Eu_{0.5}Nd_{0.5}S$ compound using the Xcrysden software package. Determine the total energy of EuS and $Eu_{0.5}Nd_{0.5}S$ as a function of volume using density functional theory to examine its ground state properties. Calculate the total energy for each volume by varying the lattice parameters. To find a minimum point, plot the values against the corresponding volumes. Analyse the energy-volume curve in figure 2(a-b) to comprehend ground state properties, such as equilibrium lattice constant (a_0), pressure derivative (B'), and bulk modulus (B_0). These data fitted by the Birch equation of state [15] using the total energies obtained from the calculations shown in Table 1. Table 1 reports these values and compares them with the existing experimental results. Figure 2(a) shows that, equilibrium energy is -22503.6721 with equilibrium volume 336.8793 for EuS and figure 2(b) show that, equilibrium energy is -42561.7726 with equilibrium volume 573.2851 for $Eu_{0.5}Nd_{0.5}S$ using TB-mBJ approximation method. Figure 3 (a-d) displays the computed electronic band structure (BS) of the EuS and Eu0.5Nd0.5S compounds. Figure 3 (a-b) demonstrates the metallic nature of the EuS compound's band structure in both spin-up and spin-down states, as the valence band and conduction band overlap each other, and the Fermi level is located at the origin. Similarity figures 3 (c-d) demonstrate that the $Eu_{0.5}Nd_{0.5}S$ compound exhibits a metallic band structure in both spin-up and spin-down states, due to the overlap of the valence band and conduction band, and the presence of the Fermi level at the origin. Therefore, the TB-mBJ approximation method clearly demonstrates the metallic nature of both compounds. This observation indicates that the electronic properties of these materials are conducive to high electrical conductivity. Additionally, the presence of overlapping bands suggests that charge carriers can easily move between the valence and conduction bands, further enhancing their metallic characteristics.

Figure 4 (a–d) displays the electronic features of EuS and $Eu_{0.5}Nd_{0.5}S$ by determining the total DOS and the partial density of states (DOS) at the Fermi level (EF). Figure 4(a-b) illustrates that the EuS compound density of state employs the TB-mBJ approximation method for both spin-up and spin-down states. Figure 4 (a) displays two peaks, one of which is approximately -0.2 eV below the Fermi level, due to the Eu-f state. The S-p state is responsible for another peak, which is approximately -4.5 eV. The Eu-d state, with a contribution from the S-p state, attributes a single peak, approximately 5.0 eV above the Fermi level. In figure 4 (b) displays two peaks in spin down state, one peak approximately -4.5 eV below the Fermi level due to S-p state. another peak approximately +4.0 eV above the fermi level due to Eu-f with small contributions of Eu-d and S-d states.

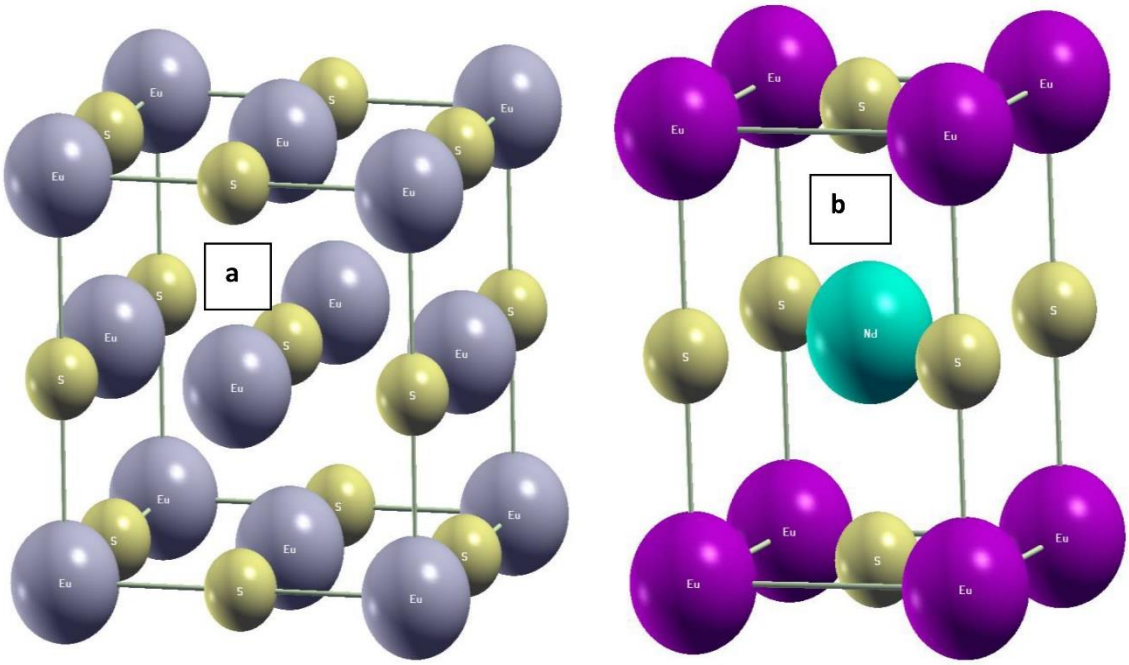

Figure 1. Unit cell structure of[a] Eus and [b] $Eu_{0.5}Nd_{0.5}S$ compounds using Xcrysden software package.

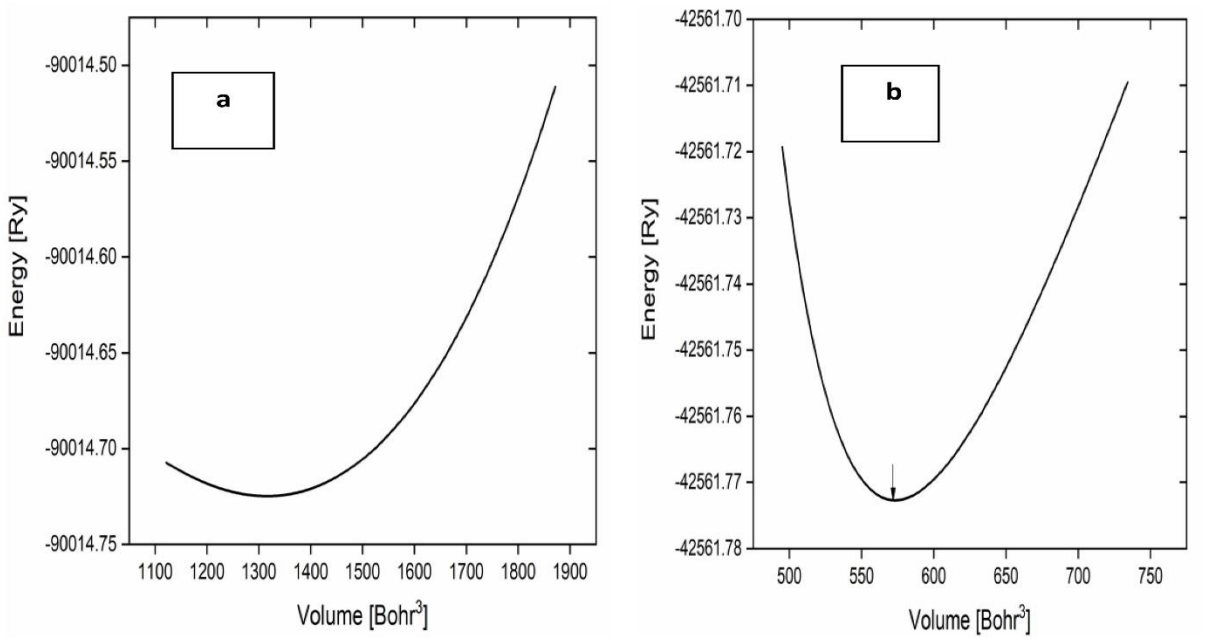

Figure 2. Equilibrium energy and Volume curve for[a] EuS and [b] $Eu_{0.5}Nd_{0.5}S$ Compounds.

Table 1. Structure Properties of EuS and $Eu_{0.5}Nd_{0.5}S$ compounds.

	EuS	$Eu_{0.5}Nd_{0.5}S$	Ref. [16-18]
Lattice parameter (Å)	$a_0=b_0=c_0$ =5.8449 Å	$a_0=b_0$=7.4458, c_0 =10.5300 Å	$a_0=b_0=c_0$ =5.7983 Å
Space group	Fm3¯m (225)	P4/mmm (123)	Fm3¯m (225)
Wyckoff position	Eu (0,0,0) S (0.5, 0.5, 0.5)	Eu (0,0,0) Nd (0.5, 0.5, 0.5) S (0, 0, 0.5)	Eu (0, 0, 0) S (0.5, 0.5, 0.5)
Bulk modulus (B) in GPa	50.3102	85.4552	52.5
Minimum Volume (V_0) in a.u^3	336.8793	573.2851	
Minimum energy (E_0) in Ry	-22503.6721	-42561.7726	
First derivative of bulk modulus (B_0) in GPa	3.6950	9.2411	

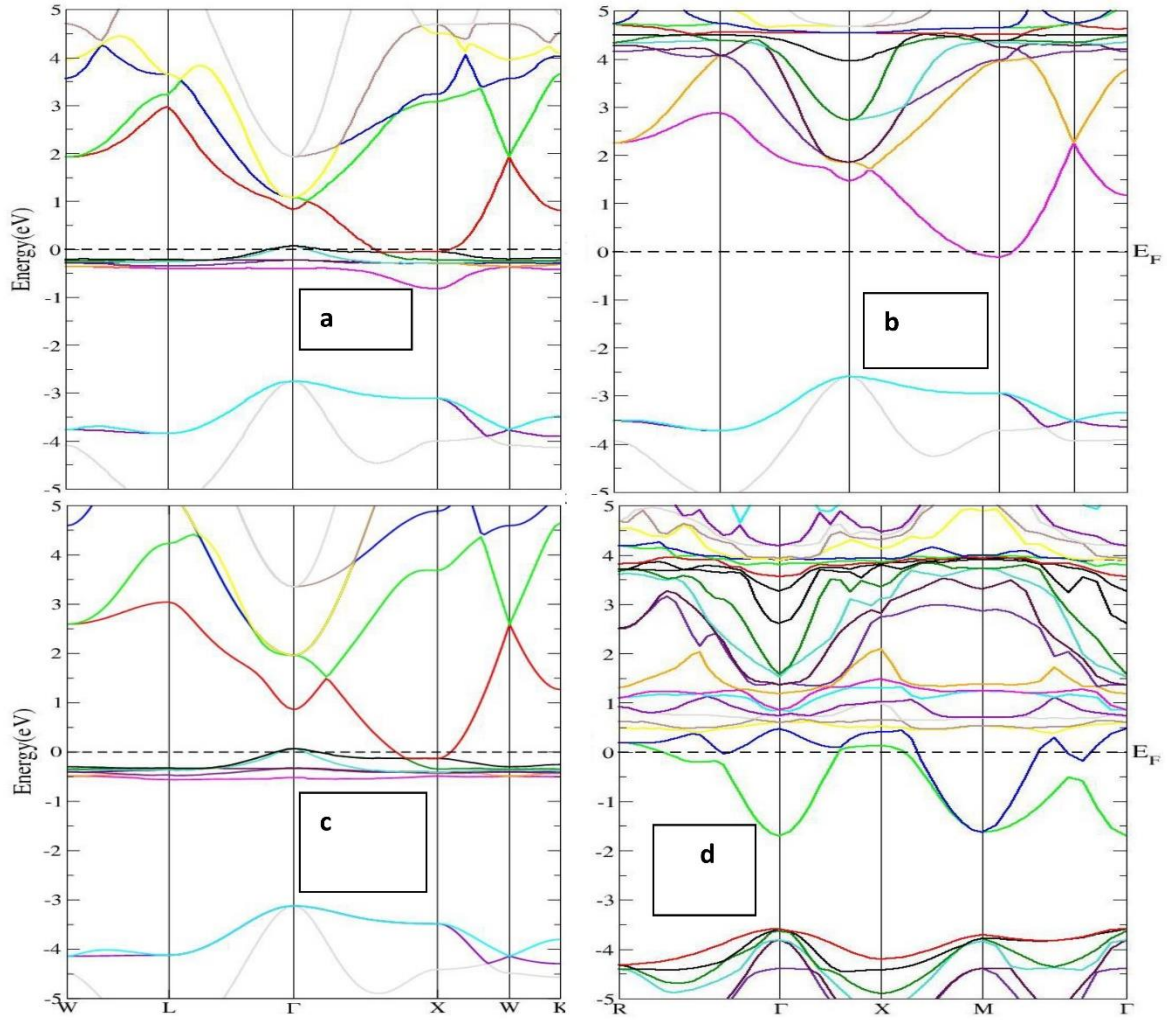

Figure 3. Band structure of (a) EuS compound with TB-mBJ spin up, (b) EuS compound with TB-mBJ spin down, (c) $Eu_{0.5}Nd_{0.5}S$ compound with TB-mBJ spin up, (d) $Eu_{0.5}Nd_{0.5}S$ compound with TB-mBJ spin down.

The third peak is approximately -4.5 eV below the Fermi level due to Nd-d and S-p states. The last peak is The $Eu_{0.5}Nd_{0.5}S$ compound density of a state is shown in figure 4(c–d). This shows that the TB-mBJ approximation method is used for both spin-up and spin-down states. Figure 4(c) displays four peaks in the spin-up state, one of which is approximately -0.2 eV below the Fermi level due to the Eu-f state. The second peak is approximately -2.2 eV below the Fermi level due to the Nd-f state.
approximately +0.5 eV above the Fermi level due to the Nd-f state. Figure 4 (d) displays three peaks in the spin-down state, one of which is approximately -4.5 eV below the Fermi level, due to the S-p state. The Nd-d state causes the second peak to rise approximately +0.5 eV above the Fermi level. The Eu-f state causes the third peak to rise approximately +4.0 eV above the Fermi level. These observations indicate a complex interplay between the different electronic states in the material, which significantly influences its overall electronic structure. Furthermore, the contribution of the rare earth elements, particularly Nd and Eu, underscores the importance of localized f-states in determining the material's electronic properties. This indicates that the electronic structure exhibits a significant difference between the spin-up and spin-down configurations, highlighting the influence of the localized f-states on the overall band structure. Such variations are crucial for understanding the material's magnetic properties and its potential applications in spintronic devices.

3.2-Magnetic and Optical properties

We have calculated magnetic properties in terms of magnetic moment. The magnetic moment shows that EuS and $Eu_{0.5}Nd_{0.5}S$ compounds are of magnetic nature. Eu-f and Nd-f state that rare earth elements are responsible for magnetic nature. These compounds exhibit unique magnetic behaviors due to the interactions between the f-electrons of the rare earth elements. Doping the Nd element effectively increases the magnetic moment. Understanding these properties can lead to advancements in materials science and potential applications in spintronics and magnetic storage devices shown in Table 2. These advancements could enable the development of more efficient data storage solutions and faster processing speeds in electronic devices. Furthermore, the exploration of other rare earth compounds may reveal additional magnetic properties, contributing to the ongoing evolution of modern technology.

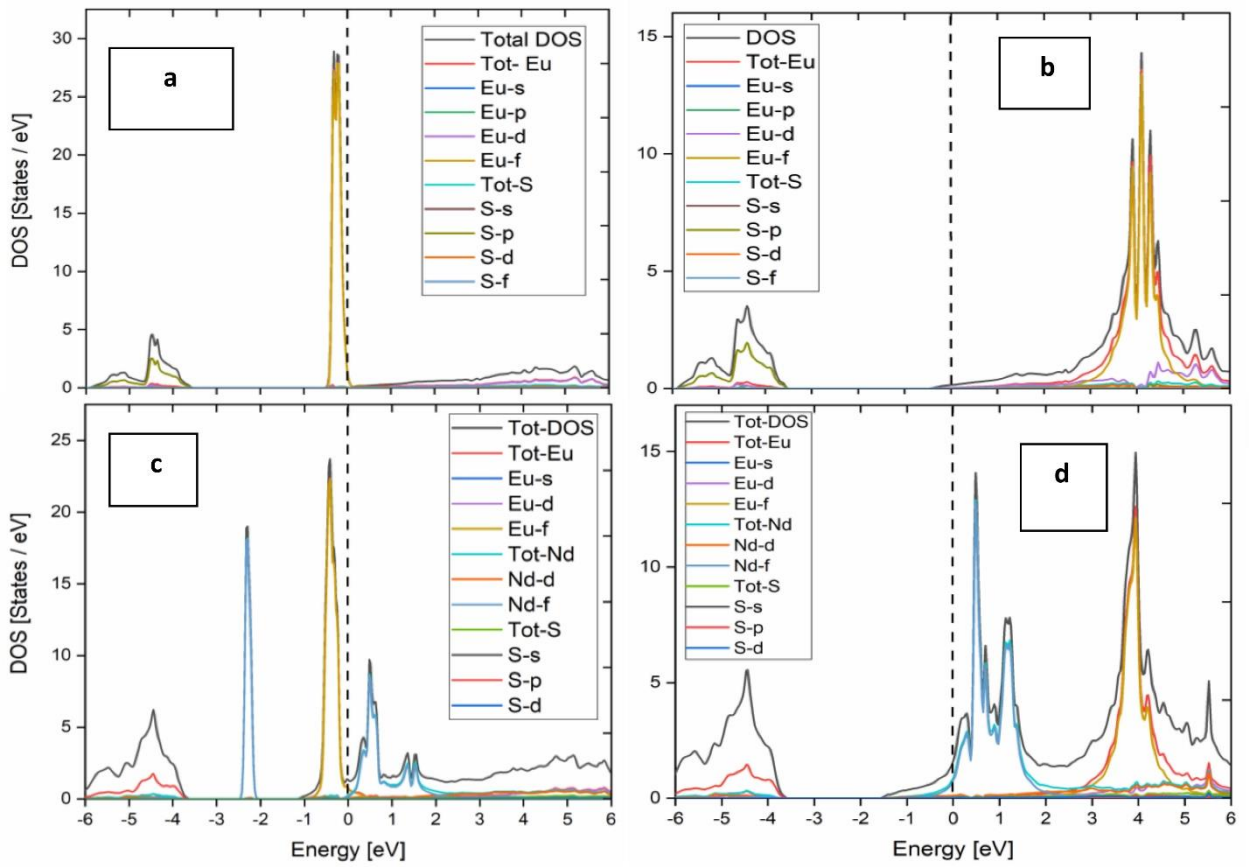

Figure 4. Total and partial Density of State of (a) EuS Spin up with TB-mBJ, (b) EuS Spin down, with TB-mBJ, (e) $Eu_{0.5}Nd_{0.5}S$ Spin up with TB-mBJ, (f) $Eu_{0.5}Nd_{0.5}S$ Spin down, with TB-mBJ.

Table-2 Magnetic moment of EuS and $Eu_{0.5}Nd_{0.5}S$

	EuS	$Eu_{0.5}Nd_{0.5}S$	Reference
Magnetic moment in Interstitial in μB	0.19954	0.65640	
Magnetic moment of Eu in μB	6.69892	6.59689	
Magnetic moment of Nd in μB	Nil	3.26829	
Magnetic moment of S in μB	0.01946	0.05864	
Total magnetic moment of Unit Cell in μB	6.91791	10.41176	LSDA +U 6.685[16]

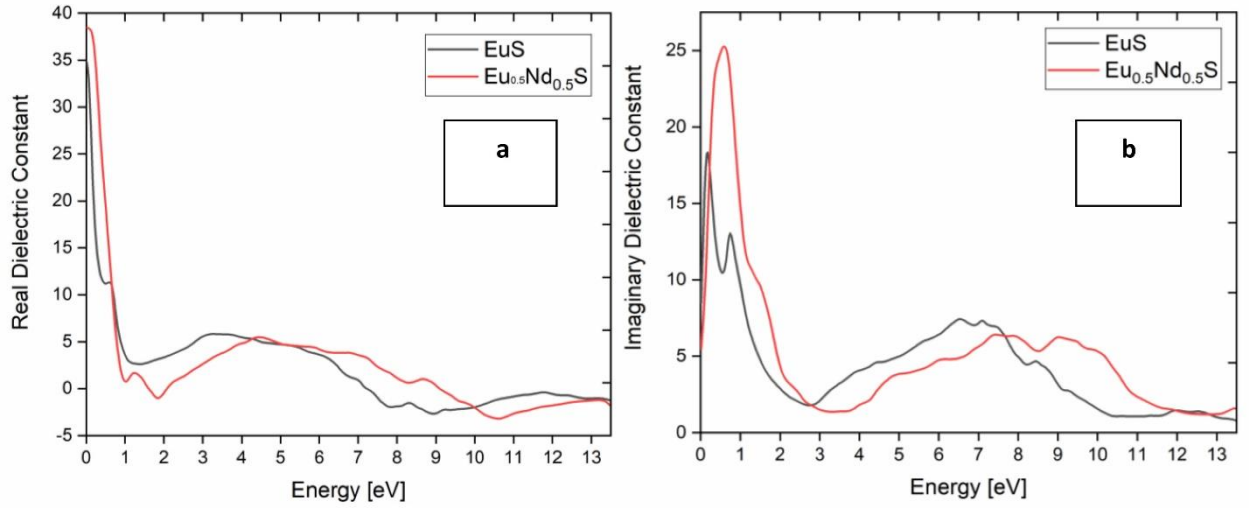

Figure 6. indicated that (a) Real dielectric Constant, (b) Imaginary dielectric constant.

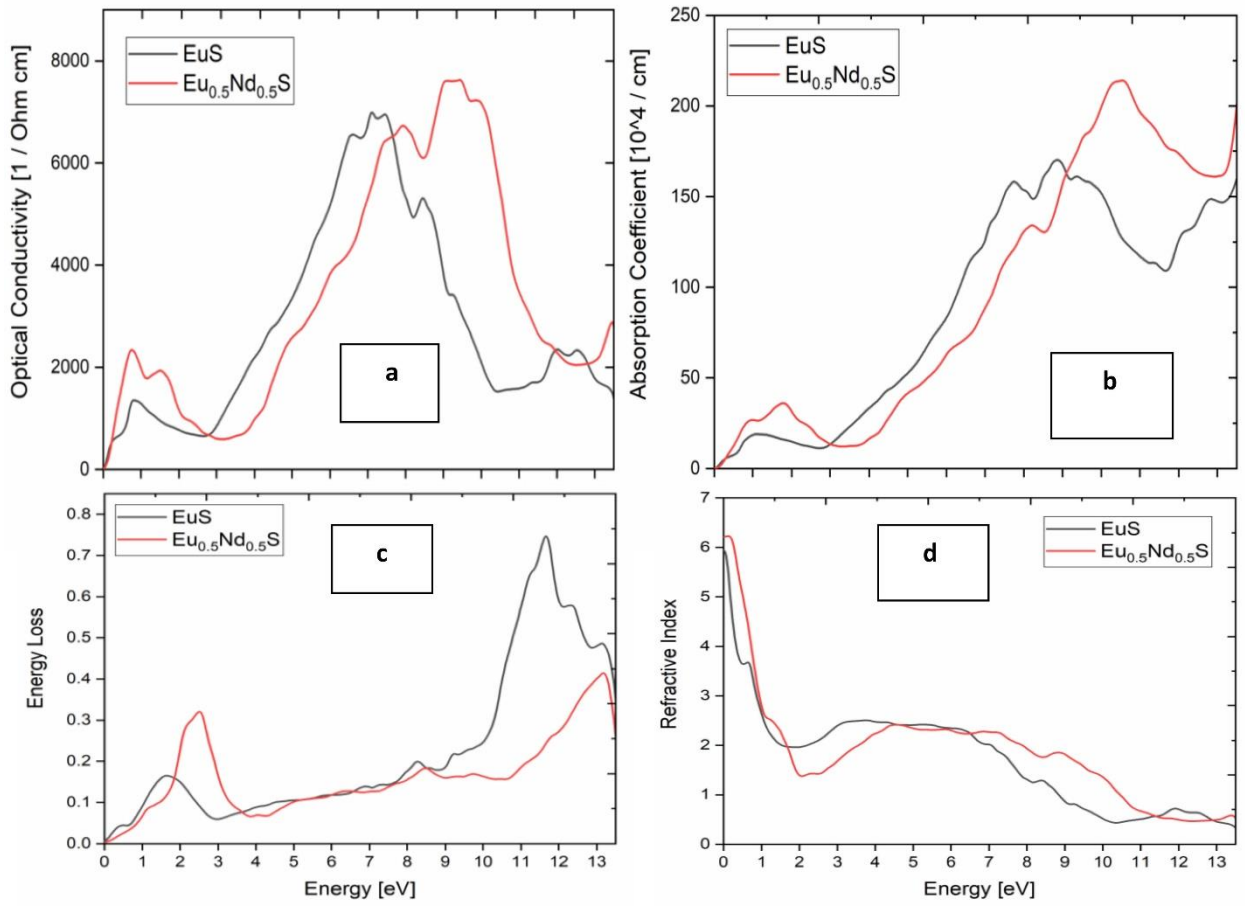

Figure 7. indicated that (a) Conductivity, (b) Absorption coefficient, (c) Optical loss and (d) Refractive index.

We have calculated optical properties in terms of dielectric constants [ε1(ω) and ε2(ω)] shown in Figure 6 (a-b), optical conductivity [σ(ω)], absorption coefficient [α(ω)], energy loss [L(ω)], and refractive index [n(ω)] shown in Figure 7 (a-d). We calculated all optical properties within the photon energy range of 0-13.5 eV. Firstly, we discuss the real dielectric constant [ε1(ω)], shown in figure 6(a), of the EuS and Eu0.5Nd0.5S compounds. In this figure, show that ε1(0) is 34 for EuS and 38 for $Eu_{0.5}Nd_{0.5}S$. This curve illustrates the negative value of the real dielectric constant at 2 eV and 10.5 eV for Eu0.5Nd0.5S, and 8 eV to 9 eV for EuS. A negative dielectric constant does indeed imply the potential for a negative refractive index, a groundbreaking property that has revolutionised our understanding of electromagnetic behaviour and led to the development of metamaterials. These materials, with their unique ability to manipulate light in ways previously thought impossible, have opened new avenues for applications in cloaking devices, superlenses, and advanced communication systems. As research continues, the exploration of such negative dielectric constants may yield even more innovative technologies that challenge conventional physics. The imaginary dielectric constant $\varepsilon_2(\omega)$ of the dielectric function for the EuS and Eu0.5Nd0.5S compound is shown in Fig. 6(b). In this figure, show that ε2(0) is 7.5 for EuS and 6.0 for $Eu_{0.5}Nd_{0.5}S$. The highest peak of $\varepsilon_2(\omega)$ is observed at 0.2 eV for EuS and 0.5 eV for $Eu_{0.5}Nd_{0.5}S$. These numbers show that the electronic properties of the two compounds are very different. EuS has a stronger dielectric response at lower energies than the doped compound. The changes in the peak locations show that the addition of Nd to the $Eu_{0.5}Nd_{0.5}S$ compound changes the band structure and the way electrons interact with each other.

Figure 7(a) illustrates the optical conductivity of the EuS and $Eu_{0.5}Nd_{0.5}S$ compounds. The optical conductivity shows one peak at 1.8 eV and a highest peak at 7.0 eV for EuS, and one peak at 1.8 eV and a highest peak at 10.0 eV for $Eu_{0.5}Nd_{0.5}S$. We find the first peak in the visible region, and the highest peak in the UV region. This indicates that the $Eu_{0.5}Nd_{0.5}S$ compound has enhanced optical properties compared to EuS, particularly in the ultraviolet range. The unique electronic structure and interactions present in the mixed compound could be responsible for these differences in optical conductivity. The absorption coefficient represents the proportion of energy absorbed as it passes through a material. It also provides information about the radiation penetration depth at a particular energy before absorption occurs. Figure 7(b) demonstrates that absorption begins at 0 eV due to the metallic properties of the materials. The absorption coefficient of $Eu_{0.5}Nd_{0.5}S$ is higher compared to EuS due to the doping of Nd. The enhanced electronic interactions and structural modifications introduced by the Nd doping are responsible for this increased absorption. As a result, materials like $Eu_{0.5}Nd_{0.5}S$ exhibit

improved performance in applications where effective energy absorption is critical, such as in photodetectors or solar cells. Figure 7(c) presents the computed energy loss function. There is the most energy loss in the EuS and $Eu_{0.5}Nd_{0.5}S$ compounds at 11.8 eV and 13.0 eV, which are the plasma resonance frequencies. This indicates that $Eu_{0.5}Nd_{0.5}S$ experiences lower energy loss compared to EuS. The minimum energy loss occurs at a specific photon energy where the trailing edges in the reflection spectra, $\varepsilon1(\omega)$ and $\varepsilon2(\omega)$, both become zero.

At the plasma frequency, the material transitions from a metallic to a dielectric response. This transition is crucial for applications in optoelectronics, as it allows for the tuning of optical properties based on the energy input. Consequently, understanding these energy loss mechanisms can lead to advancements in the design of devices that utilize $Eu_{0.5}Nd_{0.5}S$ for improved efficiency and performance in various technological applications. Figure 7(d) presents the refractive index [$n(\omega)$] for the analyzed materials, EuS and $Eu_{0.5}Nd_{0.5}S$. The static refractive index, n(0), is measured to be approximately 6.0 for EuS and 6.2 for $Eu_{0.5}Nd_{0.5}S$. In the low-energy photon region, n decreases linearly with increasing photon energy, reaching a minimum of around 10.4 eV for EuS and 11.4 eV for $Eu_{0.5}Nd_{0.5}S$. Beyond these minima, the refractive index stabilizes near a constant value around 13 eV. This behaviour suggests that the electronic transitions within these materials are significantly influenced by the composition and structural properties. Further investigation into the wavelength-dependent refractive index could provide deeper insights into the optical characteristics and potential applications of these compounds in photonic devices.

Conclusion

We employ density functional theory (DFT) to systematically investigate the optical, electronic, magnetic, and structural properties of EuS and $Eu_{0.5}Nd_{0.5}S$ compounds. The computed lattice constants and stability curves exhibit strong agreement with available experimental data, further validating the structural parameters. The electronic properties, analysed through band structure and density of states calculations, confirm the metallic nature of both compounds. Furthermore, EuS and $Eu_{0.5}Nd_{0.5}S$ exhibit intrinsic magnetic behaviour, as evidenced by their magnetic moments, which originate primarily from the Eu-f and Nd-f states. The optical analysis reveals that EuS demonstrates strong absorption in the ultraviolet (UV) region, making it a promising candidate for UV-related applications. These findings are crucial for understanding the material's magnetic interactions and its potential utility in spintronic and optoelectronic devices.

References

1. P G Steeneken, L H Tjeng, I Elfimov, G A Sawatzky, G Ghiringhelli, N B Brookes, and D-J Huang, Phys Rev Lett **88** (2002) 047201.
2. P LeClair, J K Ha, H J M Swagten, J T Kohlhepp, C H van de Vin, and W J M de Jonge, Appl Phys Lett **80** (2002) 625.
3. J P Perdew and A Zunger, Phys Rev B **23** (1981) 5048.
4. P Hohenberg and W Kohn, Phys Rev **136** (1964) B864.
5. W Kohn and P Vashishta, in Theory of the Inhomogeneous Electron Gas, eds S Lundqvist and N H March (Plenum Press, New York, 1982).
6. P Blaha, K Schwarz, G K H Madsen, D Kvasnicka, and J Luitz, WIEN2k: An Augmented Plane Wave + Local Orbitals Program for Calculating Crystal Properties, Technische Universität Wien, Austria (2001).
7. J P Perdew, K Burke, and M Ernzerhof, Phys Rev Lett **77** (1996) 3865.
8. P Blaha, K Schwarz, G K H Madsen, D Kvasnicka, and J Luitz, An Augmented Plane Wave + Local Orbitals Program for Calculating Crystal Properties (2001).
9. X Wang et al, J Alloys Compd **734** (2018) 329.
10. W Kohn, A D Becke, and R G Parr, J Phys Chem **100** (1996) 12974.
11. F D Murnaghan, Proc Natl Acad Sci USA **30** (1944) 244.
12. M Betzinger, C Friedrich, S Blügel, and A Görling, Phys Rev B **83** (2011) 045105.
13. F Murnaghan, Proc Natl Acad Sci USA **30** (1944) 244.
14. P Larson, W R L Lambrecht, A Chantis, and M van Schilfgaarde, Phys Rev B **75** (2007) 045114.
15. F Birch, Phys Rev **71** (1947) 809.
16. M Horne, P Strange, W Temmerman, Z Szotek, A Svane, and H Winter, J Phys Condens Matter **16** (2004) 5061.
17. X Zhou, K H Zhang, J Xiong, J-H Park, J H Dickerson, and W He, Size and dimensionality-dependent optical, magnetic and magneto-optical properties of binary europium-based nanocrystals: EuX (X = O, S, Se, Te) (unpublished).
18. M Schlipf, M Betzinger, M Ležaić, C Friedrich, and S Blügel, Phys Rev B **88** (2013) 094433.
19. R M Ram, A Saxena, A E Aly, and A Shankar, RSC Adv 10 (2020) 7661.
20. D H Chung, W R Buessem, F W Vahldiek, and S A Mersol, Anisotropy in Single Crystal Refractory Compounds, Vol 2 (Plenum, New York, 1968) 217–245.
21. S F Pugh, Philos Mag **45** (1954) 823.
22. L Kleinman, Phys Rev **128** (1962) 2614.
23. R H Potze and G A Sawatzky, Phys Rev B **51** (1995) 11501.